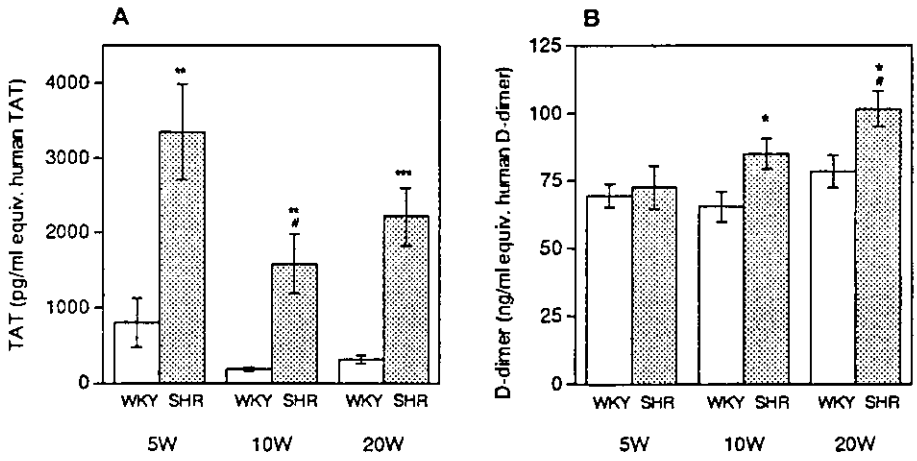

Figure 4. Thrombin–antithrombin complex (A) and D-dimer (B) levels of SHR and WKY. Plasma was obtained from SHR and WKY at different ages, and TAT and D-dimer levels were measured by ELISA. Data were expressed as equivalent to human TAT and D-dimer. *Key*: ($n = 10$) *, $P < 0.05$; **, $P < 0.01$; ***, $P < 0.001$ vs. age-matched WKY; #, $P < 0.05$ vs. each 5-week-old rats.

rarefaction and, consequently, hypoxia is induced (37,38). Hypoxia also reduces the TM expression by endothelial cells (39,40). Since exposure of endothelial cells to thrombin, a ligand of TM, decreased TM on the cell surface by internalization of thrombin–TM complex (41), enhanced coagulation seems to be one reason that the TM level on endothelial cells decreased. Cacoub et al. reported lowered plasma TM levels in hypertensive patients compared with normal subjects and suggested decreased TM expression of endothelial cells (11,13). Although no conclusive explanation for the decreased plasma TM levels was obtained in the present study, one possible mechanism by which plasma TM is reduced in hypertensive rats is through decreased TM expression of endothelial cells.

Under normal physiological conditions, vascular walls remain antithrombotic due to the presence of TM, heparan sulfate, prostacycline, and nitric oxide. Under pathogenic conditions such as inflammation, however, the antithrombotic properties of vascular walls change to prothrombotic. The decrease in TM activity on the endothelial cell surface seems to be responsible for the reduced thromboresistance of vessel walls. For example, abnormally reduced TM activity in endothelial cells has been reported in patients with homocystinuria, complicated by atherosclerosis and thrombotic disease (42), and it has been suggested that herpes simplex virus 1 may cause thrombosis by reducing TM expression and increasing tissue factor expression in humans (43). Therefore, we measured the parameters related to coagulation in order to estimate the thromboresistance of vessel walls though indirectly. Acceleration of coagulation and fibrinolytic systems indicated by the increases in TAT and D-dimer levels were observed in both SHR and DOCA-induced hypertensive rats. Clinically, Welsh et al. reported accelerated coagulation in hypertensive patients and suggested this might be due to a decrease in the antithrombotic factor of endothelial cells (44). Our findings are consistent with these reports.

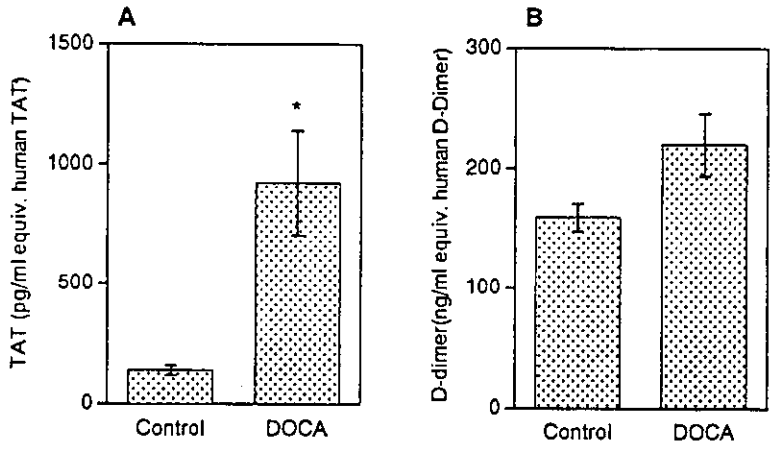

Figure 5. Thrombin–antithrombin complex (A) and D-dimer (B) levels of DOCA-induced hypertensive rats. Plasma was obtained from rats 5 weeks after the initiation of DOCA-treatment, and TAT and D-dimer levels were measured by ELISA. Data were expressed as equivalent to human TAT and D-dimer. *Key*: ($n = 7$) significantly different from control; *, $P < 0.05$.

An important question is whether hypertension induces endothelial cell damage or not. It may be difficult, however, to examine endothelial cell damage in hypertension using plasma TM levels as a marker, since hypertension may alter TM expression level of endothelial cells. Plasma TM levels could not increase as expected, even though hypertension causes endothelial cell damage, provided hypertension lowers the TM expression on endothelial cells.

In conclusion, decreased plasma TM levels and acceleration of coagulation and fibrinolytic systems were observed in both SHR and DOCA-induced hypertensive rats. These findings suggest that hypertension lowers plasma TM levels and induces a hypercoagulable state in rats.

REFERENCES

1. Esmon CT, Owen WG. Identification of an endothelial cell cofactor for thrombin-catalyzed activation of protein C. Proc Natl Acad Sci USA 1981; 78(4):2249–2252.
2. Esmon NL, Owen WG, Esmon CT. Isolation of a membrane-bound cofactor for thrombin-catalyzed activation of protein C. J Biol Chem 1982; 257(2):859–864.
3. Ishii H, Majerus PW. Thrombomodulin is present in human plasma and urine. J Clin Invest 1985; 76(6):2178–2181.
4. Ishii H, Uchiyama H, Kazama M. Soluble thrombomodulin antigen in conditioned medium is increased by damage of endothelial cells. Thromb Haemost 1991; 65(5):618–623.

5. Kazama M. Clinical evaluation of hemostatic molecular markers. Acta Haematol Jpn 1988; 51(8):1387–1394.
6. Takano S, Kimura S, Ohdama S, Aoki N. Plasma thrombomodulin in health and diseases. Blood 1990; 76(10):2024–2029.
7. Chobanian AV. 1989 Corcoran lecture: Adaptive and maladaptive responses of the arterial wall to hypertension. Hypertension 1990; 15(6 Pt 2):666–674.
8. Lee RM. Vascular changes at the prehypertensive phase in the mesenteric arteries from spontaneously hypertensive rats. Blood Vessels 1985; 22(3):105–126.
9. McCarron RM, Wang L, Siren AL, Spatz M, Hallenbeck JM. Adhesion molecules on normotensive and hypertensive rat brain endothelial cells. Proc Soc Exp Biol Med 1994; 205(3):257–262.
10. Vanhoutte PM. Endothelium and control of vascular function. Hypertension 1989; 13(6 Pt 2):658–667.
11. Cacoub P, Karmochkine M, Dorent R, Nataf P, Piette JC, Godeau P, Gandjbakhch I, Boffa MC. Plasma levels of thrombomodulin in pulmonary hypertension. Am J Med 1996; 101(2):160–164.
12. Kario K, Matsuo T, Kobayashi H, Matsuo M, Sakata T, Miyata T, Shimada K. Factor VII hyperactivity and endothelial cell damage are found in elderly hypertensives only when concomitant with microalbuminuria. Arterioscler Thromb Vasc Biol 1996; 16(3):455–461.
13. Makris T. Thrombomodulin levels in patients with arterial hypertension. Am J Med 1997; 103(4):331–332.
14. Sakamaki F, Kyotani S, Nagaya N, Sato N, Oya H, Satoh T, Nakanishi N. Increased plasma P-selectin and decreased thrombomodulin in pulmonary hypertension were improved by continuous prostacyclin thrapy. Circulation 2000; 102(22):2720–2725.
15. Erdem Y, Usalan C, Haznedaroglu IC, Altun B, Arici M, Yasavul U, Turgan C, Caglar S. Effects of angiotensin converting enzyme and angiotensin II receptor inhibition on impaired fibrinolysis in systemic hypertension. Am J Hypertens 1999; 12(11 Pt 1):1071–1076.
16. Hsu CD, Copel JA, Hong SF, Chan DW. Thrombomodulin levels in preeclampsia, gestational hypertension, and chronic hypertension. Obstet Gynecol 1995; 86(6): 897–899.
17. Naruse M, Kawana M, Hifumi S, Naruse K, Yoshihara I, Oka T, Kato Y, Monzen C, Kurimoto F, Ohsumi K, Hosoda S, Demura H. Plasma immunoreactive endothelin, but not thrombomodulin, is increased in patients with essential hypertension and ischemic heart disease. J Cardiovasc Pharmacol 1991; 17(Suppl 7):471–474.
18. Trifiletti A, Barbera N, Pizzoleo MA, Leone G, Lucifora S, Soraci S, Scamardi R, Pedulla M, Frisina N. Hemostatic disorders associated with arterial hypertension and peripheral arterial disease. J Cardio Surg 1995; 36(5):483–485.
19. Sawada K, Yamamoto H, Yago H, Suehiro S. Changes in coagulation and fibrinolytic systems of SART-stressed (repeated cold stress) animal. International J Hematol 1994; 59(Suppl 1):310 (Abstract).
20. Maruyama I, Bell CE, Majerus PW. Thrombomodulin is found on endothelium of arteries, veins, capillaries and lymphtics, and on syncytiotrophoblast of human placenta: J Cell Biol 1985; 101(2):363–371.

21. Ogura M, Ito T, Maruyama I, Saito H. Localization and biosynthesis of functional thrombomodulin in human megakaryocytes and a human megakaryoblastic cell line (MEG-01). Thromb Haemost 1990; 64(2):297–301.
22. Suzuki K, Nishioka J, Hayashi T, Kosaka Y. Functionally active thrombomodulin is present in human platelets. J Biochem (Tokyo) 1988; 104(4):628–632.
23. Pruna A, Peyri N, Berard M, Boffa MC. Thrombomodulin is synthesized by human mesangial cells. Kidney Int 1997; 51(3):687–693.
24. Harlan JM, Harker LA, Reidy MA, Gajdusek CM, Schwartz SM, Striker GE. Lipopolysaccharide-mediated bovine endothelial cell injury in vitro. Lab Invest 1983; 48(3):269–274.
25. Sawada K, Yamamoto H, Yago H, Suehiro S. A simple assay to detect endothelial cell injury; measurement of released thrombomodulin from cells. Exp Mol Pathol 1992; 57(2):116–123.
26. Smedly LA, Tonnesen MG, Sandhaus RS, Haslett C, Guthrie LA, Johnston RB Jr, Henson PM, Worthen GS. Neutrophil-mediated injury to endothelial cells: Enhancement by endotoxin and essential role of neutrophil elastase. J Clin Invest 1986; 77(4):1233–1243.
27. Kanazuka M, Shigekiyo T, Toibana N, Saito S. Increase in plasma thrombomodulin level in patients with vibration syndrome. Thromb Res 1996; 82(1):51–56.
28. Ma XL, Gao F, Nelson AH, Lopez BL, Christopher TA, Yue TL, Barone FC. Oxidative inactivation of nitric oxide and endothelial dysfunction in stroke-prone spontaneous hypertensive rats. J Pharmacol Exp Ther 2001; 298(3):879–885.
29. Ohtsuki T, Matsumoto M, Suzuki K, Taniguchi N, Kamada T. Mitochondrial lipid peroxidation and superoxide dismutase in rat hypertensive target organs. Am J Physiol 1995; 268(4 Pt 2):H1418–H1421.
30. Tse WY, Maxwell SRJ, Thomason H, Blann A, Thorpe GHG, Waite M, Holder R. Antioxidant status in controlled and uncontrolled hypertension and its relationship to endothelial damage. J Hum Hypertens 1994; 8(11):843–849.
31. Conway EM, Rosenberg RD. Tumor necrosis factor suppresses transcription of the thrombomodulin gene in endothelial cells. Mol Cell Biol 1988; 8(12):5588–5592.
32. Moore KL, Esmon CT, Esmon NL. Tumor necrosis factor leads to the internalization and degradation of thrombomodulin from the surface of bovine aortic endothelial cells in culture. Blood 1989; 73(1):159–165.
33. Nawroth PP, Handley DA, Esmon CT, Stern DM. Interleukin 1 induces endothelial cell procoagulant while suppressing cell-surface anticoagulant activity. Proc Natl Acad Sci USA 1986; 83(10):3460–3464.
34. Humbert M, Monti G, Brenot F, Sitbon O, Portier A, Grangeot-Keros L, Duroux P, Galanaud P, Simonneau G, Emilie D. Increased interleukin-1 and interleukin-6 serum concentrations in severe primary pulmonary hypertension. Am J Respir Crit Care Med 1995; 151(5):1628–1631.
35. Liu Y, Liu T, McCarron RM, Spatz M, Feuerstein G, Hallenbeck JM, Siren AL. Evidence for activation of endothelium and monocytes in hypertensive rats. Am J Physiol 1996; 270(6 Pt 2):H2125–H2131.
36. Siren AL, Heldman E, Doron D, Lysko PG, Yue TL, Liu Y, Feuerstein G, Hallenbeck JM. Release of proinflammatory and prothrombotic mediators in the

brain and peripheral circulation in spontaneously hypertensive and normotensive Wistar-Kyoto rats. Stroke 1992; 23(11):1643–1651.
37. Greene AS, Tonellato PJ, Lui J, Lombard JH, Cowley AW Jr. Microvascular rarefaction and tissue vascular resistance in hypertension. Am J Physiol 1989; 256(1 Pt 2):H126–H131.
38. Greene AS, Tonellato PJ, Zhang Z, Lombard JH, Cowley AW Jr. Effect of microvascular rarefaction on tissue oxygen delivery in hypertension. Am J Physiol 1992; 262(5 Pt 2):H1486–H1493.
39. Dufourcq P, Seigneur M, Pruvost A, Dumain P, Belloc F, Amiral J, Boisseau MR. Membrane thrombomodulin levels are decreased during hypoxia and restored by cAMP and IBMX. Thromb Res 1994; 77(3):305–310.
40. Ogawa S, Shreeniwas R, Brett J, Clauss M, Furie M, Stern DM. Effect of hypoxia on capillary endothelial cell function: modulation of barrier and coagulation function. Br J Haematol 1990; 75(4):517–524.
41. Maruyama I, Majerus PW. The turnover of thrombin-thrombomodulin complex in culture human umbilical vein endothelial cells and A549 lung cancer cells. Endocytosis and degradation of thrombin. J Biol Chem 1985; 260(29):15432–15438.
42. Rodgers GM, Conn MT. Homocysteine, an atherogenic stimulus, reduces protein C activation by arterial and venous endothelial cells. Blood 1990; 75(4):895–901.
43. Key NS, Vercellotti GM, Winkelmann JC, Moldow CF, Goodman JL, Esmon NL, Esmon CT, Jacob HS. Infection of vascular endothelial cells with herpes simplex virus enhances tissue factor activity and reduces thrombomodulin expression. Proc Natl Acad Sci USA 1990; 87(18):7095–7099.
44. Welsh CH, Hassell KL, Badesch DB, Kressin DC, Marlar RA. Coagulation and fibrinolytic profiles in patients with severe pulmonary hypertension. Chest 1996; 110(3):710–717.

Submitted February 25, 2002
Accepted August 30, 2002

Statistical Image Analysis of Cerebral Blood Flow in Vascular Dementia with Small-Vessel Disease

Takuya Yoshikawa, MD[1]; Kenya Murase, MD, PhD[2]; Naohiko Oku, MD, PhD[1]; Kazuo Kitagawa, MD, PhD[1]; Masao Imaizumi, MD[3]; Masashi Takasawa, MD[1]; Takashi Nishikawa, MD, PhD[4]; Masayasu Matsumoto, MD, PhD[1]; Jun Hatazawa, MD, PhD[3]; and Masatsugu Hori, MD, PhD[1]

[1]Department of Internal Medicine and Therapeutics, Osaka University Graduate School of Medicine, Osaka, Japan; [2]Department of Allied Health Sciences, Osaka University Graduate School of Medicine, Osaka, Japan; [3]Department of Tracer Kinetics, Osaka University Graduate School of Medicine, Osaka, Japan; and [4]Department of Clinical Neuroscience, Osaka University Graduate School of Medicine, Osaka, Japan

Small-vessel disease with dementia, which is the most frequent type of vascular dementia (VaD), often shows a cerebral blood flow (CBF) distribution with no obvious focal abnormalities and is therefore difficult to evaluate objectively. In this study, we combined CBF SPECT with 3-dimensional fractal analysis (3D-FA) to quantitatively assess the heterogeneity of CBF distribution and with 3-dimensional stereotactic surface projections (3D-SSP) to evaluate the distribution of CBF. We then evaluated the clinical validity of these techniques for the imaging diagnosis of VaD. **Methods:** The subjects consisted of 17 patients who were diagnosed as having VaD due to small-vessel disease (VaD group) on the basis of a full clinical examination, including history, neuropsychologic tests, neurologic examination, and neuroimaging methods, and 20 healthy volunteers (control group). CBF SPECT was performed with ^{99m}Tc-hexamethylpropyleneamine oxime, and the reconstructed images were subjected to image processing by 3D-FA and 3D-SSP. Based on the results, the fractal dimension (FD) was compared between the VaD and control groups, and the distribution pattern of CBF was examined in the VaD group. **Results:** The mean FD values in the VaD group and the control group were 1.093 ± 0.153 and 0.853 ± 0.062 (mean ± SD), respectively. The mean FD value in the VaD group was significantly higher than that in the control group ($P < 0.0001$). 3D-SSP analysis in the VaD group showed that there were 2 abnormal patterns: One was globally reduced blood flow in the whole cerebral cortex, and the other was a reduction mainly confined to the frontal region. **Conclusion:** CBF SPECT images showed higher mean FD values in the VaD group than in the control group, suggesting a difference in the heterogeneity of CBF. Image processing with 3D-SSP successfully revealed that reduced cortical blood flow could be divided into 2 patterns. Because image analysis techniques, such as 3D-FA and 3D-SSP, allowed the simple and objective evaluation of CBF in patients with VaD, these methods seem to be useful for detailed examination of the blood flow pattern detected by CBF SPECT in patients with VaD.

Key Words: vascular dementia; cerebral blood flow; fractal analysis; 3-dimensional stereotactic surface projections; SPECT

J Nucl Med 2003; 44:505–511

Three-dimensional assessment of cerebral blood flow (CBF) abnormality can easily be performed in daily clinical practice with SPECT, allowing us to detect the lesion of reduced CBF corresponding to the neurologic symptoms in patients with dementia before any morphologic changes are observed on CT or MRI.

Cerebral functional imaging studies of patients with vascular dementia (VaD) have revealed various findings, including patchy reduction of CBF without any specific pattern (*1*) or reduction of CBF in the frontal lobes (*2–4*). CBF abnormalities are relatively easy to detect with CBF SPECT in the case of VaD due to large cortical infarcts. But VaD is difficult to diagnose, as no diagnostic scheme has both high sensitivity and high specificity. For example, the National Institute of Neurological Disorders and Stroke–Association International pour la Recherse et l'Enseignement en Neuroscience (NINDS-AIREN) criteria (*5*) have been reported to have only 58% sensitivity and Hachinski's ischemic score (*6*) has been reported to have only 43% sensitivity with respect to pathologic diagnosis (*7*). VaD has also been classified into several subtypes. Among these subtypes, small-vessel disease with dementia is the most common VaD (*8,9*). The patients classified in the group having small-vessel disease with dementia often show no apparent focal abnormalities on CBF SPECT images. Although detecting reduced blood flow or metabolism in the cerebral cortex is important for making an early diagnosis, one cannot always detect such a reduction with visual evaluation alone. To solve this problem, more objective indices have

Received Jun. 17, 2002; revision accepted Oct. 31, 2002.

For correspondence or reprints contact: Takuya Yoshikawa, MD, Department of Internal Medicine and Therapeutics, Osaka University Graduate School of Medicine (A8), 2-2, Yamadaoka, Suita City, Osaka, 565-0871, Japan.

E-mail: yoshi@tracer.med.osaka-u.ac.jp

been introduced, such as quantification of CBF with arterial blood collection (*10*) and the accumulation ratio relative to the cerebellum. One study (*11*) showed the usefulness of semiquantitative SPECT in the diagnosis of dementia. However, it is generally difficult to quantify CBF with arterial blood collection in clinical practice because this method is invasive and requires many personnel and a long test time. The conventional region-of-interest analysis has various problems, such as acquisition of information only in the region of interest, difficulty in locating the lesion, poor reproducibility, and too much subjectivity. The recent introduction of statistical techniques for the analysis of cerebral functional images has revealed the possibility of detecting changes that are missed by conventional region-of-interest analysis. Minoshima et al. (*12,13*) have developed 3-dimensional stereotactic surface projections (3D-SSP) to map the lesions with reduced CBF in a statistical manner. However, the method is not totally free from visual inspection. Three-dimensional fractal analysis (3D-FA) is a new technique to measure the heterogeneity of CBF in a mathematic manner. In this study, we applied 3D-FA to the CBF SPECT images of patients with VaD due to small-vessel disease, which was difficult to diagnose by visual analysis. We also evaluated the spatial distribution of lesions with abnormal CBF using 3D-SSP.

MATERIALS AND METHODS

Subjects

The subjects consisted of 17 patients with VaD (6 men and 11 women; VaD group) and 20 healthy volunteers (9 men and 11 women; control group). The clinical characteristics of the subjects are shown in Table 1. They were all right-handed and underwent CBF SPECT between June 2000 and February 2002. The NINDS-AIREN criteria (*5*), the *Diagnostic and Statistical Manual of Mental Disorders* (*14*), Hachinski's ischemic score (*6*), and Erkinjuntti's criteria (*15*) were used for making the diagnosis of VaD to ensure comprehensive examination. The clinical features for VaD included sudden onset, stepwise progression, prolonged plateaus, periods of spontaneous improvement, and onset or worsening in relation to stroke or episode of hypoperfusion. The soft, focal neurologic signs or symptoms strongly supported the diagnosis of VaD. VaD subtype classifications were based on results of neuroimaging and clinical evaluation (*15*). Probable VaD was diagnosed in all 17 patients, and all were classified into the group having small-vessel disease with dementia because MRI showed small infarcts with a diameter of 3–15 mm in the basal ganglia, thalamus, pons, and deep white matter (seen as low-intensity areas on T1-weighted images and high-intensity areas on T2-weighted images), whereas there were no obvious lesions in the cortex. The 20 healthy volunteers underwent CBF SPECT for examination of vertigo or headache but had no abnormal CT or MRI findings and no evident neuropsychologic abnormalities on the basis of a full clinical examination, including history, neuropsychologic tests, and neurologic examination. The Mini-Mental State Examination (MMSE) (*16*) was performed within 3 mo of CBF SPECT to evaluate the cognitive function of the subjects.

TABLE 1
Clinical Characteristics of Control Group and VaD Group

Variable	Control group	VaD group
Subjects (*n*)	20	17
Sex (M:F)	9:11	6:11
Age (y)	62.9 ± 11.3	69.5 ± 8.5
MMSE	26.5 ± 2.6	18.6 ± 4.5

Values are mean ± SD.

In the preliminary study, we compared the heterogeneity between CBF SPECT images with ^{99m}Tc-hexamethylpropyleneamine oxime (HMPAO) and PET images with ^{18}F-FDG in another group, which consisted of 17 patients (13 men and 4 women with a mean age of 56.9 ± 14.6 y) who visited our hospital for investigation of memory impairment. ^{18}F-FDG PET has been used for imaging the demented state, in which there is a greater reduction of glucose metabolism than of blood flow. Images obtained by both ^{99m}Tc-HMPAO CBF SPECT and ^{18}F-FDG PET performed at approximately the same time (average interval, 7 d) were processed by 3D-FA to calculate the fractal dimension (FD). Informed consent was obtained from the subjects or from their families when they could not fully understand the nature and importance of the test.

Data Acquisition

^{99m}Tc-HMPAO was created by reconstituting HMPAO with 740 MBq (20 mCi) of fresh ^{99m}Tc-pertechnetate. ^{99m}Tc-HMPAO was injected intravenously while the subject rested supine on the scanning bed with the eyes closed in a quiet examination room. SPECT was done with a 4-head gamma camera (GAMMA VIEW SPECT 2000H; Hitachi Medical Corp., Tokyo, Japan), using a low-energy high-resolution parallel-hole collimator (*17*). The in-plane and axial resolution after reconstruction was 10.0 mm in full width at half maximum. SPECT acquisition was done at 8 s per step, with 128 collections over 360°, and data were recorded in a 64 × 64 matrix.

The raw SPECT data were transferred to a nuclear medicine computer (HARP 3; Hitachi Medical Corp.). The data were prefiltered with a Butterworth filter (cutoff frequency, 0.20 cycles per pixel; order, 10) and reconstructed into transaxial sections of 4.0-mm-thick images in planes parallel to the orbitomeatal line. Chang's attenuation correction was applied to the reconstructed images using an attenuation coefficient of 0.08 cm^{-1}.

PET was performed using a HEADTOME-V scanner (Shimadzu Corp., Kyoto, Japan) with a spatial resolution of 4.0 mm in full width at half maximum. The subjects rested supine on the scanning bed with the eyes closed in a quiet examination room. An individual transmission scan with a ^{68}Ge/^{68}Ga line source was obtained for each patient and used for subsequent attenuation correction of emission scan data. ^{18}F-FDG (370 MBq) was injected intravenously, and after 45 min, data were acquired over a scanning period of 20 min using a 128 × 128 matrix. The final slice thickness was 3.125 mm.

3D-FA

In this study, fractal analysis was used to assess the heterogeneity of SPECT images. Fractal geometry allows structures to be quantitatively characterized in geometric terms even if their form is irregular and fragmented, because fractal geometry deals with the geometry of hierarchies and random processes. This type of analysis is most useful for characterizing branching structures,

such as the pulmonary airways and blood vessels (*18,19*). Spatial changes of regional blood flow and metabolism in living organs are measurable using fractal analysis with PET and SPECT (*20–23*). Studies have shown that the observed variance increases along with the number of subregions studied in an organ (*20*) and that such resolution-dependent variance can be described by fractal analysis (*20,23,24*). Studies have also shown that biologic systems display considerable spatial and temporal heterogeneity, such as heterogeneity in CBF, myocardial blood flow, and pulmonary blood flow (*24–28*).

In fractal geometry, the relationship between a measure (M) and the scale (a) is expressed as:

$$M(a) = k \cdot a^{-D}, \qquad \text{Eq. 1}$$

where k is a scaling constant and D is called the FD (*18*).

The cutoff value for the maximum radioactivity was set at 11 levels from 35% to 50% at equal intervals on the reconstructed images, and the number of voxels with a radioactivity exceeding the cutoff value was calculated in each case. The cutoff value of the maximal radioactivity was defined as a and the total number of voxels measured was defined as M (a), as shown in Equation 1. Then, the number of voxels and the cutoff value were transformed into natural logarithms and their relationship was graphed. The graph was drawn with the logarithm of the cutoff value on the horizontal axis and that of the number of voxels with a radioactivity above the cutoff on the vertical axis. The slope of the regression line on this graph corresponded to the FD.

3D-SSP

3D-SSP created with the Neurological Statistical Image Analysis Software (NEUROSTAT) developed by Minoshima et al. (*12,13*) from the University of Washington were used to evaluate the spatial distribution of abnormal CBF. One study on cerebral glucose metabolism measured by PET showed that metabolism was reduced in the posterior part of the cingulate gyrus before changes were detected at other sites in patients with very early Alzheimer's disease (AD) (*29*). These changes at various sites have come to be detected more easily and objectively with 3D-SSP. NEUROSTAT anatomically normalizes the individual SPECT data to the standard brain and compares the regional voxel data with the normal SPECT database, calculating the z score ([normal mean − individual value]/normal SD) for each voxel of the cerebral surface, and displays the sites at which voxel value is statistically reduced. For anatomic standardization, a reference line (the line connecting the anterior commissure and posterior commissure) was detected and was transferred to the coordinate system of the standard brain according to the Talairach–Tournoux atlas (*30*). The individual image was then transformed to fit the standard brain through linear and nonlinear transformation. 3D-SSP extracts 3-dimensional functional information from the gray matter using pixels preset to cover the whole brain surface after the brain image of each subject is transformed to the standard brain image through anatomic standardization. Normalization was performed by whole-brain counting.

Statistical Analysis

The significance of differences in the FD value between the control group and the VaD group was assessed by the Mann–Whitney test. Correlations between CBF SPECT and ^{18}F-FDG PET images were determined by calculating Spearman rank correlation. Results were expressed as mean ± SD, and statistical significance was defined as $P < 0.01$.

RESULTS

The age and sex ratios did not significantly differ between the VaD group and the control group, though the control group consisted of younger subjects than did the VaD group. The MMSE score of the VaD group was 18.6 ± 4.5 (mean ± SD), which was significantly lower than the score of 26.5 ± 2.6 found for the control group. Figure 1 shows a 62-y-old woman who underwent examination for memory impairment. Fractal analysis was performed on her CBF SPECT and ^{18}F-FDG PET images, and the FD value was determined to be 1.109 for the ^{18}F-FDG PET image and 1.278 for the CBF SPECT image. Although the number of voxels with a count exceeding a specific threshold differed between the 2 images, the lines corresponding to the FD were parallel and had almost the same gradient. When we compared FD data between ^{99m}Tc-HMPAO CBF SPECT and ^{18}F-FDG PET images (Fig. 2), a significant correlation was shown by Spearman rank correlation analysis (r = 0.619; $P < 0.01$), suggesting that ^{99m}Tc-HMPAO CBF SPECT images may show similar heterogeneity to ^{18}F-FDG PET images.

Figure 3 shows T2-weighted MR images, SPECT images, and 3D-SSP images of representative subjects from the control and VaD groups. The VaD patient has multiple small, bilateral infarcts in the basal ganglia on the T2-weighted MR image, diffuse reduction of CBF on the SPECT and PET images, and a reduction mainly confined to the frontal region on the 3D-SSP image. Figure 4 compares FD data between the VaD and control groups. The mean FD

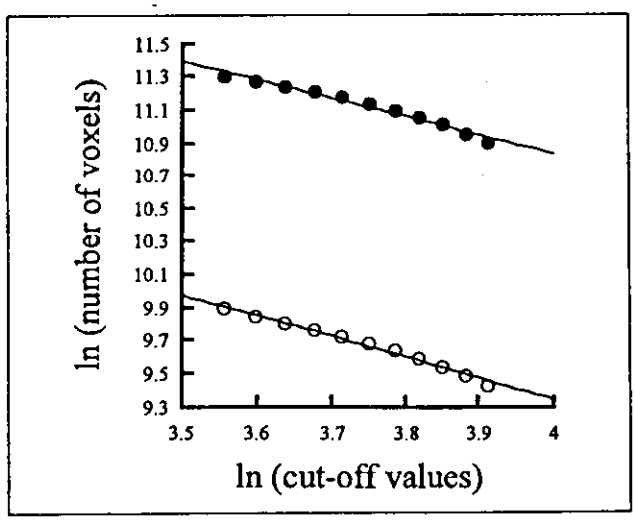

FIGURE 1. Comparison of FD calculated for ^{99m}Tc-HMPAO CBF SPECT image and FD calculated for ^{18}F-FDG PET image of 62-y-old woman who underwent examination for memory impairment. Horizontal axis shows natural logarithm of cutoff values, and vertical axis shows natural logarithm of number of voxels in area surrounded by contour obtained with radioactivity above cutoff value. Slope of regression line on this graph corresponds to FD. ● = FD value for ^{18}F-FDG PET image ($y = -1.109x + 15.29$; $r = 0.988$); ○ = FD value for ^{99m}Tc-HMPAO CBF SPECT image ($y = -1.278x + 14.46$; $r = 0.995$).

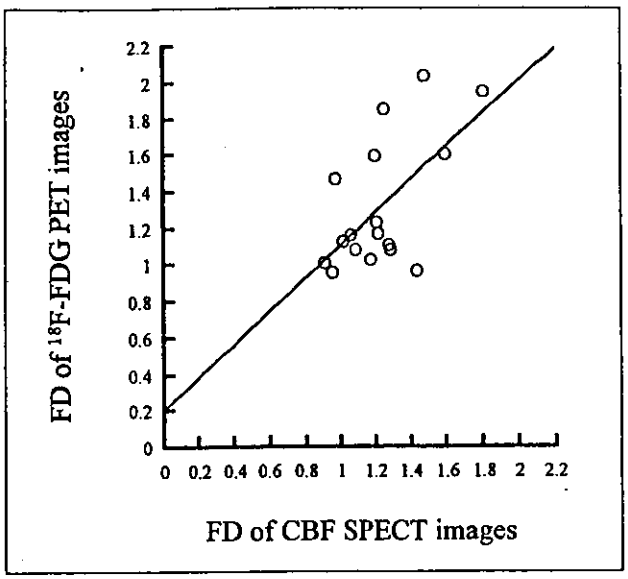

FIGURE 2. Scatter plots of FD data between ^{99m}Tc-HMPAO CBF SPECT and ^{18}F-FDG PET images in VaD group. Spearman rank correlation analysis showed significant correlation between FDs of the 2 images ($y = 0.902x + 0.211$; $r = 0.619$; $P < 0.01$).

values of the VaD and control groups were 1.093 ± 0.153 and 0.853 ± 0.062, respectively, showing a significant difference between the 2 groups ($P < 0.0001$). In addition, the VaD group was divided into 2 groups based on an MMSE score of 20, and we then compared the mean FD values among the control group, the VaD group with a mild MMSE score decline (MMSE ≥ 20, $n = 10$), and the VaD group with a moderate to severe MMSE score decline (MMSE < 20, $n = 7$) (Fig. 4). When divided at the FD value of 0.977 (mean + 2 SDs in the control group), the control group and the VaD group with a moderate to severe MMSE score decline (MMSE < 20) could be clearly separated.

Table 2 lists the individual age, sex, FD value, MMSE score, and sites of reduced blood flow on the 3D-SSP z score maps of the 17 patients in the VaD group. The z score maps showed that the reduction of CBF in VaD could be divided into 2 abnormal patterns: global reduction and a decrease in the frontal region only. Figure 5 shows representative 3D-SSP z score maps from patients with a global reduction of CBF (patient 1, Fig. 5A) and with reduction confined to the frontal region of CBF (patient 8, Fig. 5B). The image of reduced CBF in the frontal region was obtained from the same subject as shown in Figure 3.

DISCUSSION

VaD is one of the major diseases responsible for senile dementia. Dementia is relatively difficult to diagnose in persons with an MMSE score of 20–25. The borderlines among so-called age-related cognitive impairment, mild cognitive impairment that is considered as the transition to the initial stage of dementia, and dementia itself remain unclear (*31*). A patient with VaD due to small-vessel disease may well be difficult to differentiate from a healthy volunteer by neuroimaging studies, but such a patient would presumably not resemble a healthy volunteer clinically. Cerebral functional imaging techniques that have been used to assist in diagnosis, such as PET and SPECT, are helpful for understanding the pathology of VaD. However, evaluation based only on morphologic criteria should be considered with caution, as demonstrated by the report of Loeb et al. (*32*) that CT showed no differences in the site and size of cerebral infarction between demented and nondemented groups.

PET is superior to SPECT with respect to sensitivity and spatial resolution. PET images obtained with ^{18}F-FDG have been widely used for the diagnosis of AD because of a higher spatial resolution than those obtained with ^{15}O gas or $H_2{}^{15}O$. A correspondence between ^{99m}Tc-HMPAO SPECT and ^{18}F-FDG PET has been found in AD (*33*). In this study, before 3D-FA was applied to CBF SPECT images, the FD

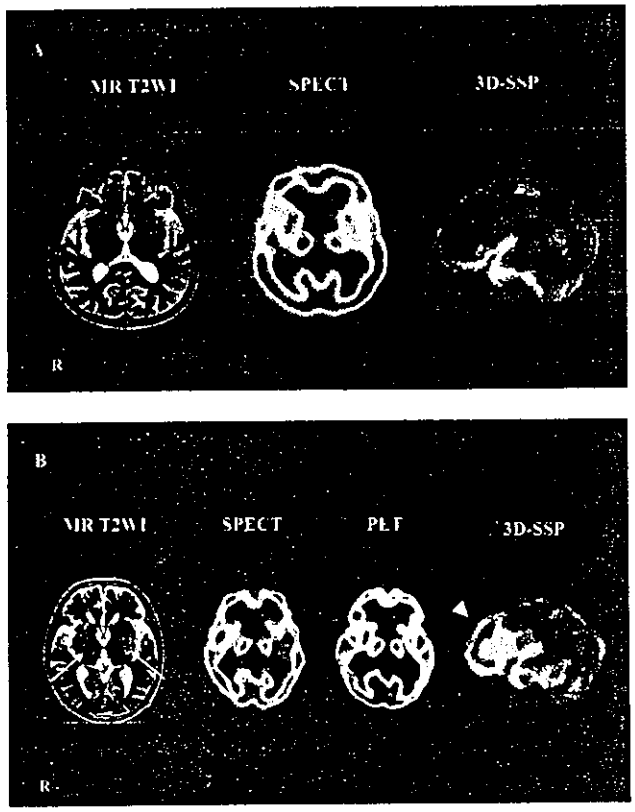

FIGURE 3. T2-weighted MR images (left), SPECT or PET images (center), and 3D-SSP images (right) of representative subjects from control and VaD groups. (A) Images of 70-y-old man from control group. His FD was 0.799, and his MMSE score was 29. (B) Images of 75-y-old man from VaD group. His FD was 1.151, and his MMSE score was 15. In VaD, T2-weighted MR images revealed multiple small, bilateral infarcts in basal ganglia (arrows), SPECT and PET images showed diffuse decrease in CBF, and 3D-SSP image showed reduction mainly confined to frontal region (arrowhead). T2WI = T2-weighted image.

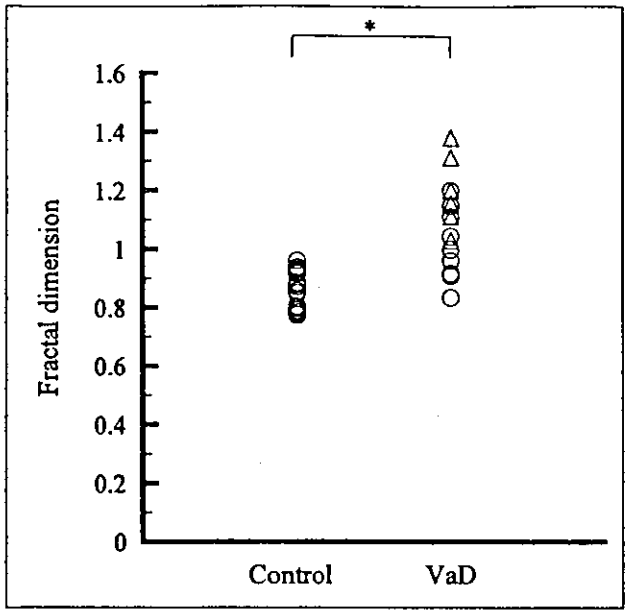

FIGURE 4. Comparison of FD between control group (n = 20) and VaD group (n = 17). Mann–Whitney test showed significant difference in FD between the 2 groups ($P < 0.0001$). Δ = 7 patients with VaD at MMSE score of less than 20. *$P < 0.0001$.

value obtained from images processed by 3D-FA was examined for its correlation with that obtained from similarly processed ^{18}F-FDG PET images. The FD value obtained from the former images correlated significantly with that from the latter images, suggesting that the heterogeneity of accumulation was similar on both ^{99m}Tc-HMPAO CBF SPECT and ^{18}F-FDG PET images. This finding indicates that the FD value determined by ^{99m}Tc-HMPAO CBF SPECT images may also reflect cerebral metabolism and that SPECT can be used at medical institutions not equipped for PET.

TABLE 2
Clinical Characteristics of Each VaD Patient

Patient no.	Age (y)	Sex	FD	MMSE	Decreased CBF
1	57	M	0.912	23	Diffuse
2	82	F	1.199	20	Frontal
3	67	F	1.029	19	Diffuse
4	67	F	1.373	10	Frontal
5	74	F	1.108	21	Diffuse
6	69	F	0.963	21	Diffuse
7	69	F	0.835	22	Diffuse
8	75	M	1.151	15	Frontal
9	87	M	1.307	11	Diffuse
10	55	F	0.916	22	Diffuse
11	64	F	0.995	23	Diffuse
12	75	M	0.995	23	Diffuse
13	62	F	1.145	20	Diffuse
14	79	F	1.108	19	Frontal
15	63	F	1.042	21	Diffuse
16	66	M	1.307	10	Diffuse
17	71	M	1.199	17	Frontal

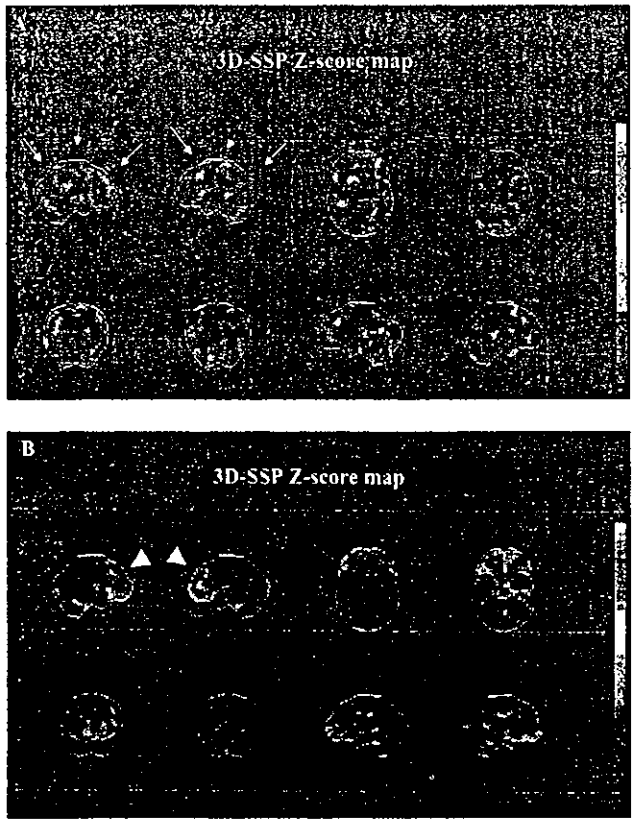

FIGURE 5. Representative 3D-SSP z score maps from patients with diffuse reduction of CBF and reduction mainly confined to frontal region of CBF. (A) Diffuse reduction of CBF (arrows) (patient 1). (B) Decrease in frontal region (arrowheads) (patient 8).

Many studies have examined the cerebral metabolic dynamics of VaD using functional imaging techniques (*34,35*). One study showed reduced CBF and a reduced cerebral metabolic rate of oxygen in the white matter and cortex of patients with Binswanger's disease, a clinical type of VaD (*36*). Other SPECT studies have shown that CBF was diffusely reduced (*1*) or that it was mainly reduced in the frontal lobes of patients with VaD (*2–4*). Thus, the findings have varied and no definite conclusions have been obtained. Cerebral blood flow and metabolism are generally reduced at sites of cerebrovascular damage. In patients with dementia, reduced CBF and metabolism may not be limited to the sites of cerebrovascular damage but may extend to wider areas. The 17 patients in the VaD group had small-vessel disease with dementia, according to the VaD classification of NINDS-AIREN (*5*). Small-vessel disease with dementia includes multiple lacunar strokes and Binswanger's disease. Other types in the VaD classification include multi-infarct dementia characterized by extensive infarcts in the cortex and frequent dementia symptoms; hypoperfusion; hemorrhagic dementia; and, less frequently, strategic single-infarct dementia, which were not examined in the present study. Although CBF SPECT is generally

evaluated visually, visual detection of CBF heterogeneity or other CBF distribution abnormalities in VaD due to small-vessel disease is often difficult. Therefore, CBF SPECT images were statistically analyzed to assess the heterogeneity and distribution of CBF in the present study.

CBF SPECT images of the VaD group were quantitatively more heterogeneous and had a higher FD value than those of the control group. Nagao et al. reported that AD patients showed a more heterogeneous CBF than did healthy volunteers (*26*). The mean FD values for the healthy volunteers and AD patients were 0.52 ± 0.09 and 0.74 ± 0.33, respectively, with a significant difference between the 2 groups. The difference in the FD value of the control group between studies was probably due to different settings of the Butterworth filter for pretreatment (cutoff frequency, 0.25 cycles per pixel). It is necessary to compare the heterogeneity of CBF in VaD and AD to examine whether the 2 diseases can be distinguished by the FD value.

We also used 3D-SSP to evaluate CBF distribution in patients with VaD. A line of 6 pixels directed from the surface into the brain is set for each site on the brain surface, and the highest pixel count is used as the value for that site. Therefore, 3D-SSP could be used in patients with VaD due to small-vessel disease who had no cortical infarction but, instead, had infarcts in the perforator vessel system. Although it is difficult to visually detect reduced blood flow in VaD on ordinary orbitomeatal line tomograms, the changes could be delineated with 3-dimensional cerebral surface images in 8 projections. 3D-SSP z score mapping revealed 2 patterns of reduced CBF, a global reduction and a reduction confined to the frontal region (Table 2). For example, patient 4 showed a high FD value of 1.373 and heterogeneous CBF. The 3D-SSP z score map showed reduced CBF in the frontal region, with an MMSE score of 10. This result is consistent with previous reports that CBF was reduced diffusely with no specific pattern in VaD (*1*) or, conversely, that CBF was reduced in the frontal lobes (*2–4*). In contrast to AD, VaD often shows reduced blood flow in the anterior region. In fact, 5 of our 17 patients had reduced blood flow mainly in the frontal region. Although not examined in the present study, symptoms associated with frontal lobe dysfunction have been reported in patients with VaD (*37*). Attention should be paid to differentiation from frontotemporal dementia (*38*) or Parkinson's disease with dementia, which resemble VaD with respect to reduced blood flow in the frontal region. The 17 patients with VaD due to small-vessel disease even showed reduced blood flow in the cortex, with no morphologic abnormalities. This finding indicates that the statistical image analysis could detect reduced CBF, which was probably due to functional impairment as a remote effect (diaschisis) secondary to the disconnection between the deep cerebrum and cortex (*39,40*). Although the data are not presented here, a comparison of the VaD and control groups showed a global reduction in CBF on 3D-SSP in the VaD group.

Voxel-by-voxel analytic techniques may be sensitive to image quality, which may reflect differences in instruments and imaging conditions. The FD value is influenced by the collimator type and the image reconstitution filters. Therefore, a database of images should carefully be created under the same conditions. A database of normal images has to be constructed to prepare diagnostic statistical images for comparison with images from patients. In preparing such a normal database, one needs to determine to what extent the definition of "normal" and the parameters of the database should be unified, including number of subjects, age, sex, radioactive agent used, imaging devices and conditions, and method of reconstruction. Although it is desirable to prepare a normal database with images taken from age-matched healthy volunteers for each age group, it was impossible to collect a sufficient number of such images for the present study.

CONCLUSION

The present study suggested that the FD value calculated by 3D-FA may be an objective index of the heterogeneity of CBF in VaD and may be useful for easily and objectively evaluating VaD patients and healthy volunteers. In addition, the use of 3D-SSP allowed clearer visualization of the CBF distribution in VaD. Statistical image-analysis methods to enhance the determination of etiology are promising tools to characterize the CBF pattern in VaD, which is not easy to diagnose through conventional visual analysis.

ACKNOWLEDGMENTS

We thank Yukio Nakamura, Hiroaki Matsuzawa, Kouichi Fujino, and Tomoko Fukunaga for helping us to perform the nuclear medicine examinations and for evaluating cognitive function.

REFERENCES

1. Deutsch G, Tweedy JR. Cerebral blood flow in severity-matched Alzheimer and multi-infarct patients. *Neurology.* 1987;37:431–438.
2. Jagust WJ, Bundinger TF, Reed BR. The diagnosis of dementia with single photon emission computed tomography. *Arch Neurol.* 1987;44:258–262.
3. Tohgi H, Chiba K, Sasaki K, Hiroi S, Ishibashi Y. Cerebral perfusion patterns in vascular dementia of Binswanger type compared with senile dementia of Alzheimer type: a SPECT study. *J Neurol.* 1991;238:365–370.
4. Starkstein SE, Sabe L, Vazquez S, et al. Neuropsychological, psychiatric, and cerebral blood flow findings in vascular dementia and Alzheimer's disease. *Stroke.* 1996;27:408–414.
5. Roman GC, Tatemichi TK, Erkinjuntti T, et al. Vascular dementia: diagnostic criteria for research studies—report of the NINDS-AIREN International Workshop. *Neurology.* 1993;43:250–260.
6. Hachinski VC, Iliff LD, Zilhka E, et al. Cerebral blood flow in dementia. *Arch Neurol.* 1975;32:632–637.
7. Gold G, Giannakopoulos P, Junior C, et al. Sensitivity and specificity of newly proposed clinical criteria for possible vascular dementia. *Neurology.* 1997;49: 690–694.
8. Tatemichi TK, Desmond DW, Paik M, et al. Clinical determinants of dementia related to stroke. *Ann Neurol.* 1993;33:568–575.
9. Meyer JS, Xu G, Thornby J, Chowdhury MH, Quach M. Is mild cognitive impairment prodromal for vascular dementia like Alzheimer's disease? *Stroke.* 2002;33:1981–1985.
10. Hatazawa J, Iida H, Shimosegawa E, Sato T, Murakami M, Miura Y. Regional cerebral blood flow measurement with iodine-123-IMP autoradiography: normal

values, reproducibility and sensitivity to hypoperfusion. *J Nucl Med.* 1997;38: 1102–1108.
11. Bonte FJ, Tintner R, Weiner MF, Bigio EH, White CL. Brain blood flow in the dementias: SPECT with histopathologic correlation. *Radiology.* 1993;186:361–365.
12. Minoshima S, Frey KA, Koeppe RA, Foster NL, Kuhl DE. A diagnostic approach in Alzheimer's disease using three-dimensional stereotactic surface projections of fluorine-18-FDG PET. *J Nucl Med.* 1995;36:1238–1248.
13. Minoshima S, Koeppe RA, Frey KA, et al. Anatomic standardization: linear scaling and nonlinear warping of functional brain images. *J Nucl Med.* 1994;35: 1528–1537.
14. American Psychiatric Association. *Diagnostic and Statistical Manual of Mental Disorders.* 4th ed. Washington, DC: American Psychiatric Association; 1994: 143–146.
15. Erkinjuntti T, Inzitari D, Pantoni L, et al. Research criteria for subcortical vascular dementia in clinical trials. *J Neural Transm Suppl.* 2000;59:23–30.
16. Folstein MF, Folstein SE, McHugh PR. "Mini-mental state": a practical method for grading the cognitive state of patients for the clinician. *J Psychiatr Res.* 1975;12:189–198.
17. Kimura K, Hashikawa K, Etani H, et al. A new apparatus for brain imaging: four-head rotating gamma camera single photon emission computed tomograph. *J Nucl Med.* 1990;31:603–609.
18. Mandebrot BB. *Fractal Geometry of Nature.* San Francisco, CA: W.H. Freeman and Company; 1982:131–137.
19. Weibel ER. Fractal geometry: a design principle for living organisms. *Am J Physiol.* 1991;261:361–369.
20. Kuikka JT, Tiihonen J, Karhu J. Fractal analysis of striatal dopamine re-uptake sites. *Eur J Nucl Med.* 1997;24:1085–1090.
21. Kuikka JT, Bassingthwaighte JB, Henrich MM, Feinendegen LE. Mathematical modeling in nuclear medicine. *Eur J Nucl Med.* 1991;18:351–362.
22. Kuikka JT. Effect of tissue heterogeneity on quantification in positron emission tomography. *Eur J Nucl Med.* 1995;22:1457–1458.
23. Kuikka JT, Yang J, Karhu J, et al. Imaging the structure of the striatum: a fractal approach to SPECT image interpretation. *Physiol Meas.* 1998;19:367–374.
24. Bassingthwaighte JB, King RB, Roger SA. Fractal nature of regional myocardial blood flow heterogeneity. *Circ Res.* 1989;65:578–590.
25. Barman SA, McCloud LL, Catravas JD, Ehrhart IC. Measurement of pulmonary blood flow by fractal analysis of flow heterogeneity in isolated canine lungs. *J Appl Physiol.* 1996;81:2039–2045.
26. Nagao M, Murase K, Kikuchi T, et al. Fractal analysis of cerebral blood flow distribution in Alzheimer's disease. *J Nucl Med.* 2001;42:1446–1450.
27. Nagao M, Murase K, Yasuhara Y, Ikezoe J. Quantitative analysis of pulmonary emphysema: three-dimensional fractal analysis of single-photon emission computed tomography images obtained with a carbon particle radioaerosol. *AJR.* 1998;171:1657–1663.
28. Murase K, Nagao M, Kikuchi T. Three-dimensional fractal analysis for quantification of heterogeneity of radioisotope distribution in the organ using SPECT [abstract]. *J Nucl Med.* 1999;40(suppl):292P.
29. Minoshima S, Giordani B, Berent S, Frey KA, Foster NL, Kuhl DE. Metabolic reduction in the posterior cingulate cortex in very early Alzheimer's disease. *Ann Neurol.* 1997;42:85–94.
30. Talairach J, Tournoux P. *Co-Planar Stereotaxic Atlas of the Human Brain: 3-Dimensional Proportional System: An Approach to Cerebral Imaging.* New York, NY: Thieme Medical Publishers; 1988.
31. Ritchie K, Touchon J. Mild cognitive impairment: conceptual basis and current nosological status. *Lancet.* 2000;355:225–228.
32. Loeb C, Gandolfo C, Croce R, Conti M. Dementia associated with lacunar infarction. *Stroke.* 1992;23:1225–1229.
33. Herhoz K, Schopphoff H, Schmidt M, et al. Direct comparison of spatially normalized PET and SPECT scans in Alzheimer's disease. *J Nucl Med.* 2002; 43:21–26.
34. Frackowiak RS, Pozzilli C, Legg NJ, et al. Regional cerebral oxygen supply and utilization in dementia: a clinical and physiological study with oxygen-15 and positron tomography. *Brain.* 1981;104:753–778.
35. Mielke R, Pietrzyk U, Jacobs A, et al. HMPAO SPET and FDG PET in Alzheimer's disease and vascular dementia: comparison of perfusion and metabolic pattern. *Eur J Nucl Med.* 1994;21:1052–1060.
36. Yao H, Sadoshima S, Kuwabara Y, Ichiya Y, Fujishima M. Cerebral blood flow and oxygen metabolism in patients with vascular dementia of the Binswanger type. *Stroke.* 1990;21:1694–1699.
37. Wolfe N, Linn R, Babikian VL, Knoefel JE, Albert ML. Frontal systems impairment following multiple lacunar infarcts. *Arch Neurol.* 1990;47:129–132.
38. The Lund and Manchester Groups. Clinical and neuropathological criteria for frontotemporal dementia. *J Neurol Neurosurg Psychiatry.* 1994;57:416–418.
39. Kobayashi S, Okada K, Yamashita K. Incidence of silent lacunar lesion in normal adults and its relation to cerebral blood flow and risk factors. *Stroke.* 1991;22: 1379–1383.
40. Hatazawa J, Shimosegawa E, Satoh T, Toyoshima H, Okudera T. Subcortical hypoperfusion associated with asymptomatic white matter lesions on magnetic resonance imaging. *Stroke.* 1997;28:1944–1947.

J Neurol (2003) 250 : 194–200
DOI 10.1007/s00415-003-0972-9

ORIGINAL COMMUNICATION

Quantification of the heterogeneity of cerebral blood flow in vascular dementia

Takuya Yoshikawa
Kenya Murase
Naohiko Oku
Kazuo Kitagawa
Masao Imaizumi
Masashi Takasawa
Piao Rishu
Kazuo Hashikawa
Takashi Nishikawa
Masatsugu Hori
Masayasu Matsumoto

Received: 20 June 2002
Received in revised form:
10 September 2002
Accepted: 16 September 2002

Takuya Yoshikawa, MD (✉) · N. Oku · K. Kitagawa · M. Takasawa · P. Rishu · K. Hashikawa · M. Hori · M. Matsumoto
Department of Internal Medicine and Therapeutics
Osaka University Graduate School of Medicine (A8)
2-2, Yamadaoka, Suita City
Osaka, 565-0871, Japan
Tel.: +81-6/6879-3461
Fax: +81-6/6879-3469
E-Mail: yoshi@tracer.med.osaka-u.ac.jp

K. Murase
Department of Allied Health Sciences
Osaka University Graduate School of Medicine
Osaka, Japan

M. Imaizumi
Department of Tracer Kinetics
Osaka University Graduate School of Medicine
Osaka, Japan

T. Nishikawa
Department of Clinical Neuroscience
Osaka University Graduate School of Medicine
Osaka, Japan

Abstract *Background* In vascular dementia (VaD), assessment of cerebral blood flow by single photon emission computed tomography (CBF SPECT) has been used to detect a patchy decrease of blood flow or a frontal reduction. In addition to reduced blood flow, the heterogeneous distribution of cerebral blood flow is often observed in VaD. However, no objective method to evaluate the heterogeneity has been established. In this study, we applied three-dimensional fractal analysis (3D-FA) to CBF SPECT images as a method for assessing the heterogeneity of the cerebral blood flow distribution in VaD. *Subjects and Methods* The subjects included 18 patients with a diagnosis of VaD (aged 69.7 ± 8.3) based on neuropsychological testing and imaging findings and 18 age-matched controls (aged 66.9 ± 10.3). CBF SPECT images were obtained with ^{99m}Tc-hexamethyl propyleneamine oxime. On the reconstructed images, we obtained a linear regression equation between the cut-off values (from 35 to 50%) and the number of voxels with a radioactivity exceeding the cut-off value transformed into natural logarithms, and then calculated the fractal dimension from the slope of the regression line thus obtained. The Mini-Mental State Examination (MMSE) was used to evaluate cognitive function. *Results* The fractal dimensions were 1.084 ± 0.153 and 0.853 ± 0.062 (mean ± SD) in the VaD and control groups, respectively. The fractal dimension was significantly greater in the VaD group than in the control group ($p < 0.0001$). A significant negative correlation was observed between the fractal dimension and the MMSE score in the VaD group ($r = 0.871$, $p < 0.0001$). *Conclusions* Because the CBF SPECT images of VaD patients showed a higher fractal dimension, these images were quantitatively more heterogeneous than those of age-matched controls. In the VaD group, cognitive function was shown to decline as the fractal dimension increased and images became more heterogeneous.

Key words cerebral blood flow · dementia · tomography · cerebrovascular disorders

JON 972

Introduction

The progressive aging of the population has made it important to assess the status of dementia and to decide an appropriate therapeutic strategy. Vascular dementia (VaD) and Alzheimer's disease (AD) are common causes of dementia. VaD is one of the main complications of cerebrovascular disease, and its early diagnosis has attracted attention because prevention and treatment are possible.

Measurement of cerebral blood flow by single photon emission computed tomography (CBF SPECT) using ^{99m}Tc labeled tracers allows us to easily assess cerebral dysfunction on the basis of three-dimensional images. Using this method, reduced blood flow or changes of metabolism corresponding to neurological symptoms can be found before morphological changes are detected by X ray computed tomography (CT) or magnetic resonance imaging (MRI).

Previous studies have found various imaging patterns related to cerebral function in VaD patients, such as a patchy decrease of blood flow [1] or reduced blood flow in the frontal lobes [2–4]. However, this reduced blood flow is not necessarily specific for VaD. CBF SPECT images are usually evaluated visually. CBF SPECT can be useful to detect cortical hypofunction in cases where small vessel disease is so relatively mild as to be of uncertain relevance to the cognitive impairment, but it is not always possible to do so with visual evaluation alone. To assess reduced blood flow or metabolism objectively, several techniques have been introduced, including quantitative determination of cerebral blood flow (CBF) with arterial blood collection [5] and calculation of the accumulation ratio relative to the cerebellum. It has also been reported that semi-quantitative SPECT may be useful for diagnosing dementia [6]. It is known that CBF shows a less uniform distribution in VaD patients than that in normal individuals [1, 7–8]. It has been reported that reduced CBF is related to cognitive impairment in VaD [9–11]. Defining a single index of heterogeneity of CBF distribution is the first step to test its usefulness in the auxiliary diagnosis of VaD and evaluation of its progression.

Heterogeneity of radioisotope distribution provides us with useful information for diagnosis of functional status of organs and tissues. In this study, fractal analysis was used to assess the heterogeneity of SPECT images. Fractal analysis is a mathematical technique for dealing with complex structures that have no characteristic length scale (scale-invariant) [12]. Fractal geometry allows structures to be quantitatively characterized in geometric terms even if their form is irregular and fragmented, because fractal geometry deals with the geometry of hierarchies and random processes. The hypothesis can be explored that fractal geometry serves as a design principle in biological organisms. This type of analysis is most useful for characterizing branching structures, such as the pulmonary airways and blood vessels [13–14]. Scale-invariant systems are usually characterized by noninteger dimensions called "fractal" dimensions. Spatial changes of regional blood flow and metabolism in living organs are measurable by using fractal analysis with positron emission tomography (PET) and SPECT [12, 15–17]. It has been previously shown that the observed variance increases along with the number of subregions studied in an organ [12], and such resolution-dependent variance can be described by fractal analysis [12, 17, 18]. Numerous studies have shown that biological systems show considerable spatial and temporal heterogeneity, such as cerebral blood flow, myocardial blood flow and pulmonary blood flow [18–20]. In the present study, three-dimensional fractal analysis (3D-FA) was applied to CBF SPECT images to examine its usefulness for assessing the heterogeneity of CBF distribution in the VaD of small-vessel disease.

Subjects and methods

Subjects

The subjects were 18 VaD patients, including 6 men and 12 women (VaD group), and 18 age-matched controls who comprised 5 men and 13 women (Control group). The clinical characteristics of the subjects are shown in Table 1. All of the subjects are right-handed. The VaD patients underwent CBF SPECT between June 2000 and July 2001. The diagnosis of VaD was based on the following standards: the National Institute of Neurological Disorders and Stroke-Association International pour la Recherche et l'Enseignement en Neuroscience (NINDS-AIREN) [21] classification. Diagnostic and Statistical Manual of Mental Disorders (DSM-IV) [22], Hachinski's ischemic score [23], and Erkinjuntti's criteria [24]. All 18 patients were diagnosed as having probable VaD, which were categorized as having vascular dementia due to small-vessel disease according to the NINDS-AIREN classification. In the basal ganglia, thalamus, pons, and deep white matter of these patients without any obvious lesions in the cortex, MRI revealed multiple small infarcts (≧3 mm but ≦15 mm in diameter), which appeared hypointense on T1-weighted images and hyperintense on T2-weighted images. The age-matched controls were 18 individuals who underwent ^{99m}Tc-hexamethyl propyleneamine oxime (^{99m}Tc-HMPAO) SPECT for the investigation of dizziness or headache, and had no abnormalities on CT or MRI as well as no neurological abnormalities. The Mini-Mental State Examination (MMSE) [25] was performed to evaluate cognitive function within 3 months of the SPECT examination. Patients who could not perform the intellectual

Table 1 Clinical characteristics of age-matched controls and patients with vascular dementia

variable	Control	VaD
No. of cases	18	18
Sex, M:F	5:13	6:12
Age, y	66.9±10.3	69.7±8.3
MMSE	26.5±2.6	18.8±4.4

Values are shown as mean ± SD
VaD vascular dementia; *M* male; *F* female; *MMSE* Mini-Mental State Examination

function test, such as those with aphasia, and other non-evaluable patients, were excluded. Informed consent was obtained from the subjects when possible. Informed consent was also obtained from the families of any VaD patients who could not fully understand the nature and objective of the examinations.

Data Acquisition

^{99m}Tc-HMPAO was created by reconstituting HMPAO with 20 mCi (740 MBq) of fresh ^{99m}Tc pertechnetate. ^{99m}Tc-HMPAO was injected intravenously while the subject rested supine on the scanning bed with the eyes closed in a quiet examination room. SPECT scanning was done with a four-headed gamma camera (GAMMA VIEW SPECT 2000H, Hitachi Medical Corp., Tokyo, Japan), using a low-energy high-resolution parallel-hole collimator [26]. The in-plane and axial resolution after reconstruction was 10.0 mm in full width at half maximum (FWHM). SPECT acquisition was done at 8 seconds per step, with 128 collections over 360°, and data were recorded using a 64×64 matrix.

The raw SPECT data were transferred to a nuclear medicine computer (HARP 3, Hitachi Medical Corp., Tokyo, Japan). The data were prefiltered with a Butterworth filter (cut-off frequency: 0.20 cycles/pixel, order 10) and transaxial sections were used to reconstruct 4.0 mm thick images in planes parallel to the orbitomeatal line. Chang's attenuation correction was applied to the reconstructed images using an attenuation coefficient of 0.08 cm^{-1}.

Fractal Analysis

As described previously [27, 28], familiar matrices from classical geometry such as length, area, and volume depend on the scale at which we decide to examine an object. In fractal geometry, the relationship between a measure (M) and the scale (a) is expressed as

$$M(a) = k \cdot a^{-D}, \qquad \text{Equation 1.}$$

where k is a scaling constant and D is called the fractal dimension [13].

The cut-off value for the maximum radioactivity was set at 11 levels from 35 to 50 % at equal intervals on the reconstructed images and the number of voxels with a radioactivity exceeding the cut-off value was calculated in each case (Fig. 1). The cut-off value of the maximal radioactivity was defined as a and the total number of voxels measured was defined as M (a), as shown in Equation 1. Then the number of voxels and the cut-off value were transformed into natural logarithms and their relationship was graphed. The graph was drawn with the logarithm of the cut-off value on the horizontal axis and that of the number of the voxels with a radioactivity above the cut-off on the vertical axis. The slope of the regression line on this graph corresponded to the fractal dimension (Fig. 2).

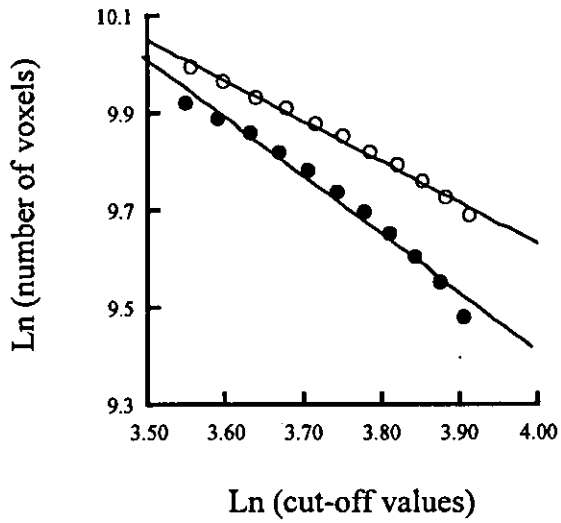

Fig. 2 Method of calculating the fractal dimension. The graph is drawn with the natural logarithm of the cut-off values on the horizontal axis and that of the number of the voxels in the area surrounded by the contour obtained with radioactivity above the cut-off value on the vertical axis. The slope of the regression line on this graph corresponds to the fractal dimension. ○; age-matched control ($y = -0.846x + 13.01$; $r = 0.997$). ●; a patient with vascular dementia ($y = -1.199x + 14.20$; $r = 0.989$).

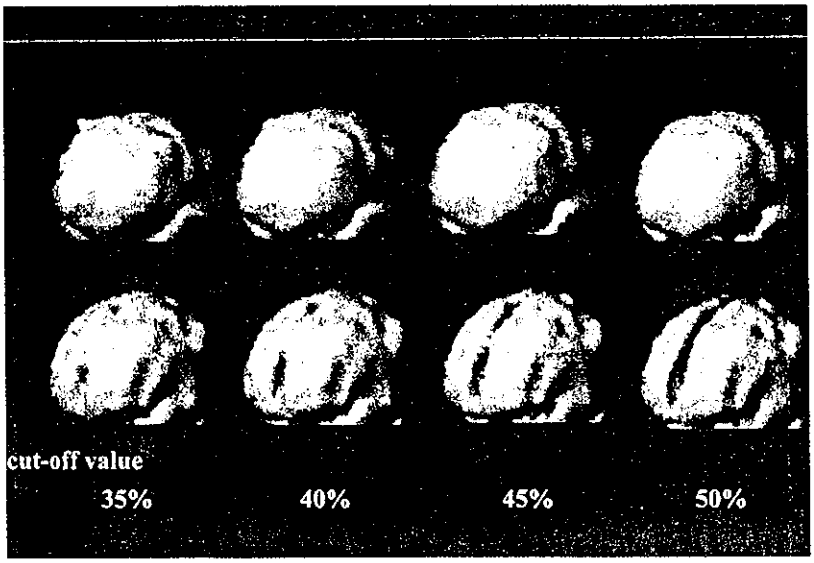

Fig. 1 Comparison of three-dimensional surface rendering of SPECT images using different cut-off values. The cut-off values shown from the left are 35, 40, 45, and 50 %. Upper: The image of the age-matched control. Lower: The image of a patient with vascular dementia. In the patient with vascular dementia, the heterogeneity of cerebral blood flow becomes greater with an increase of the cut-off value.

Statistical Analysis

The significance of differences in the fractal dimension between the control group and the VaD group was assessed by the Mann-Whitney U test. Correlations between the fractal dimension and the MMSE score were determined by calculating Spearman's rank correlation. Results are expressed as the mean ± SD and statistical significance was defined as $p < 0.01$.

Results

There was no significant difference between the VaD group and the control group with regard to age and gender distribution. The MMSE score was 18.8 ± 4.4 (mean ± SD) in the VaD group, which was significantly lower, compared with 26.5 ± 2.6 in the control group. The cognitive impairment was found in the VaD group. Fig. 3 shows representative T2-weighted MRI, SPECT images, and surface rendering of SPECT images from the control group and the VaD group. These cases are the same subjects as shown in Fig. 1 and 2.

Fig. 4 shows a comparison between the VaD group and the control group. The fractal dimension of the VaD group and the control group was 1.084 ± 0.153 and 0.853 ± 0.062, respectively, with a significant difference being found between the two groups ($p < 0.0001$).

Fig. 5 shows the correlation between the fractal dimension and the MMSE score in the VaD group. The fractal dimension increased as the MMSE score decreased (i. e., as cognitive impairment became more severe) and a significant negative correlation was observed between the fractal dimension and the MMSE score ($r = 0.871$; $p < 0.0001$).

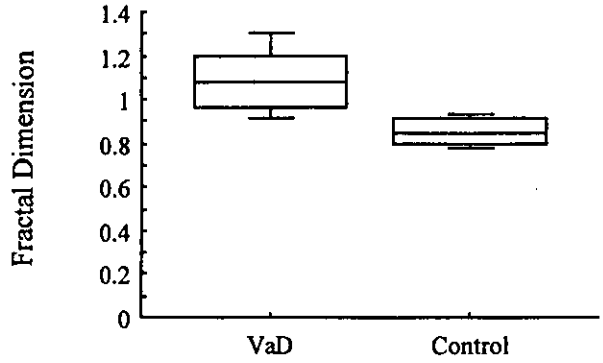

Fig. 4 Comparison of the fractal dimension between the control group and the vascular dementia group. A significant difference was found between the two groups ($p < 0.0001$) by the Mann-Whitney U test. *$p < 0.0001$

Discussion

Many studies have assessed the cerebral circulation and metabolism in VaD patients using PET and SPECT. One study with CT showed no difference in the location and size of infarcts between the groups with and without dementia, suggesting that evaluation of morphological findings alone should be done carefully [29]. One study of PET in Binswanger's disease, a clinical variant of VaD, revealed a decrease of CBF and the cerebral metabolic rate for oxygen in the white matter and cortex [30]. Other studies with SPECT have shown that CBF was diffusely reduced [1], or that blood flow was mainly reduced in the frontal lobe [2–4]. Thus, no definite conclusions have been reached about the cerebral circulation and metabolism in VaD. CBF SPECT images are usually evaluated visually, but it is often difficult to visually de-

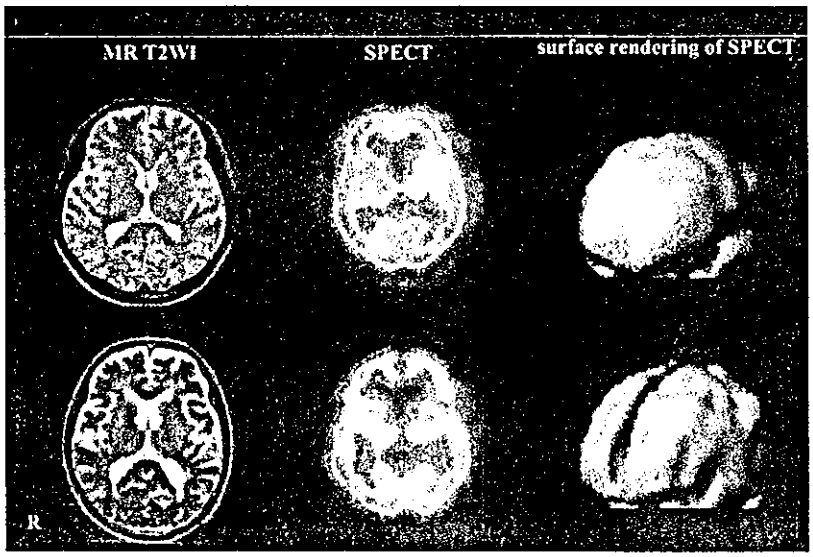

Fig. 3 MR T2WI, SPECT, and surface rendering of SPECT images of representatives from each of the control and vascular dementia groups. Upper row; A 66-year-old man from the control group. His fractal dimension was 0.846 and the MMSE score was 29. Lower row: A 71-year-old man from the vascular dementia group. His fractal dimension was 1.199 and the MMSE score was 17. In vascular dementia, MR T2WI revealed multiple small infarcts in the basal ganglia on both sides, and SPECT showed a diffuse decrease of cerebral blood flow.
MR T2WI; T2-weighted MRI, R; right, MMSE; Mini-Mental State Examination

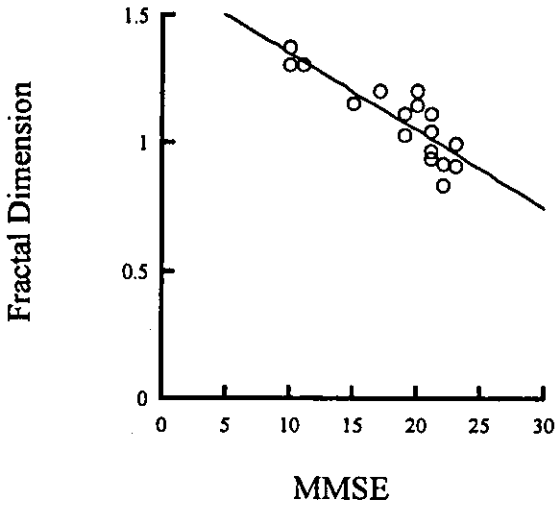

Fig. 5 Scatter plot of the fractal dimension and Mini-Mental State Examination (MMSE) scores in the vascular dementia group. A significant correlation was found between the fractal dimension and the MMSE score ($y = -0.03x + 1.651$; $r = 0.871$; $p < 0.0001$) by Spearman's rank correlation analysis.

tect the heterogeneous distribution of CBF in VaD of the small-vessel disease type. We compared the fractal dimension between the VaD and control groups in the present study. Because the CBF SPECT images of VaD patients showed a higher fractal dimension, these images were quantitatively more heterogeneous than those of age-matched controls. One study [31–34] that examined the cerebral circulation and metabolism in small-vessel disease patients showed that the decrease of mean CBF in patients with a morphologically normal cortex is presumed to be due to hypofunction secondary to disconnection between the deep cerebrum and the cortex. This finding suggests that the heterogeneity of CBF distribution in VaD may reflect reduced blood flow over a wider area than that affected on CT and MRI due to diaschisis of regions with neural connections to the ischemic focus.

To assess the clinical significance of fractal dimension data, its relationship with the MMSE was examined in our VaD patients. It has been suggested that reduced CBF may be related to cognitive impairment [9–11]. Although cognitive impairment is thought to occur when the hippocampus, thalamus, or temporal lobe is damaged, no definite site has been identified. It has also been reported that not only the site of damage, but also the volume of the brain involved is related to cognitive impairment [35]. In the present study, fractal analysis of CBF SPECT images was performed for the whole brain and not for a specific region. The result was a significant negative correlation between the fractal dimension and the MMSE score ($r = 0.871$; $p < 0.0001$). Although the data are not presented here, there was no statistically significant correlation between the average accumulation calculated semi-quantitatively instead of the CBF and the MMSE score in the VaD group.

Since statistical techniques have recently been used in the analysis of functional brain images, it has become possible to detect changes that were previously missed by regions of interest (ROI) analysis. Statistical parametric mapping (SPM) [36] transforms PET or SPECT images to standard cerebral images and allows three-dimensional statistical analysis of the images in a voxel-by-voxel manner. Use of three-dimensional stereotaxic surface projections (3D-SSP) [37] allows the easier and more objective detection of the extent of lesions in the functional brain imaging of AD patients.

The statistical techniques may detect differences in images caused by the camera and the imaging conditions. The type of collimator used for improving both sensitivity and resolution in detecting γ rays emitted from the body or the type of the image reconstruction filter may affect the fractal dimension. Therefore, a database should be prepared by taking various images under the same conditions. The important factor in calculating the fractal dimension from SPECT images is the cut-off value. The cut-off value for the maximum radioactivity was set at 11 levels from 35 to 50% at equal intervals and the number of voxels with a radioactivity exceeding the cut-off value was calculated in each case. In all cases, the relationship between the cut-off value and the number of voxels transformed into natural logarithms became linear, suggesting that the cut-off values used in this analysis were reasonable.

VaD and AD are two representative causes of senile dementia. In contrast with VaD, AD has been considered to be associated with reduced blood flow in the posterior cerebral region as compared with the anterior region [38]. To clinically apply the concept of 3D-FA, we will separately determine the fractal dimensions of the anterior and posterior regions in patients with VaD and AD, and will examine whether it is possible to distinguish VaD from AD based on the region of reduced cerebral blood flow. 3D-FA does not depend on the equipment used and provides an objective index of the heterogeneity of CBF.

Acknowledgments We thank Mr. Yukio Nakamura and Miss Tomoko Fukunaga for their technical support during our work.

References

1. Deutsch G, Tweedy JR (1987) Cerebral blood flow in severity-matched Alzheimer and multi-infarct patients. Neurology 37:431–438
2. Jagust WJ, Bundinger TF, Reed BR (1987) The diagnosis of dementia with single photon emission computed tomography. Arch Neurol 44:258–262
3. Tohgi H, Chiba K, Sasaki K, Hiroi S, Ishibashi Y (1991) Cerebral perfusion patterns in vascular dementia of Binswanger type compared with senile dementia of Alzheimer type: a SPECT study. J Neurol 238:365–370
4. Starkstein SE, Sabe L, Vazquez S, Teson A, Petracca G, Chemerinski E, Di Lorenzo G, Leiguarda R (1996) Neuropsychological, psychiatric, and cerebral blood flow findings in vascular dementia and Alzheimer's disease. Stroke 27:408–414
5. Hatazawa J, Iida H, Shimosegawa E, Sato T, Murakami M, Miura Y (1997) Regional cerebral blood flow measurement with iodine-123-IMP autoradiography: normal values, reproducibility and sensitivity to hypoperfusion. J Nucl Med 38:1102–1108
6. Bonte FJ, Tintner R, Weiner MF, Bigio EH, White CL (1993) Brain blood flow in the dementias: SPECT with histopathologic correlation. Radiology 186:361–365
7. Frackowiak RS, Pozzilli C, Legg NJ, Du Boulay GH, Marshall J, Lenzi GL, Jones T (1981) Regional cerebral oxygen supply and utilization in dementia. A clinical and physiological study with oxygen-15 and positron tomography. Brain 104:753–778
8. Mielke R, Pietrzyk U, Jacobs A, Fink GR, Ichimiya A, Kessler J, Herholz K, Heiss WD (1994) HMPAO SPET and FDG PET in Alzheimer's disease and vascular dementia: comparison of perfusion and metabolic pattern. Eur J Nucl Med 21:1052–1060
9. Hachinski VC, Lassen NA, Marshall J (1974) Multi-infarct dementia. A cause of mental deterioration in the elderly. Lancet 2:207–210
10. Kitagawa Y, Meyer JS, Tachibana H, Mortel KF, Rogers RL (1984) CT-CBF correlations of cognitive deficits in multi-infarct dementia. Stroke 15:1000–1009
11. Ballard C, O'Brien J, Morris CM, Barber R, Swann A, Neill D, Mckeith I (2001) The progression of cognitive impairment in dementia with Lewy bodies, vascular dementia and Alzheimer's disease. Int J Geriatr Psychiatry 16:499–503
12. Kuikka JT, Tiihonen J, Karhu J (1997) Fractal analysis of striatal dopamine re-uptake sites. Eur J Nucl Med 24:1085–1090
13. Mandebrot BB (1982) Fractal geometry of nature. Freeman WH, San Francisco, pp 131–137
14. Weibel ER (1991) Fractal geometry: a design principle for living organisms. Am J Physiol 261:361–369
15. Kuikka JT, Bassingthwaighte JB, Henrich MM, Feinendegen LE (1991) Mathematical modeling in nuclear medicine. Eur J Nucl Med 18:351–362
16. Kuikka JT (1995) Effect of tissue heterogeneity on quantification in positron emission tomography. Eur J Nucl Med 22:1457–1458
17. Kuikka JT, Yang J, Karhu J, Laitinen T, Tupala E, Hallikainen T, Tiihonen J (1998) Imaging the structure of the striatum: a fractal approach to SPECT image interpretation. Physiol Meas 19:367–374
18. Bassingthwaighte JB, King RB, Roger SA (1989) Fractal nature of regional myocardial blood flow heterogeneity. Circ Res 65:578–590
19. Barman SA, McCloud LL, Catravas JD, Ehrhart IC (1996) Measurement of pulmonary blood flow by fractal analysis of flow heterogeneity in isolated canine lungs. J Appl Physiol 81:2039–2045
20. Nagao M, Murase K, Kikuchi T, Ikeda M, Nebu A, Fukuhara R, Sugawara T, Miki H, Ikezoe J (2001) Fractal Analysis of Cerebral Blood Flow Distribution in Alzheimer's Disease. J Nucl Med 42:1446–1450
21. Roman GC, Tatemichi TK, Erkinjuntti T, Cummings JL, Masdeu JC, Garcia JH, Amaducci L, Orgogozo JM, Brun A, Hofman A (1993) Vascular dementia: diagnostic criteria for research studies. Report of the NINDS-AIREN International Workshop. Neurology 43:250–260
22. American Psychiatric Association (1994) Diagnostic and Statistical Manual of Mental Disorders, Fourth Edition. Washington DC: American Psychiatric Association
23. Hachinski VC, Iliff LD, Zilhka E, Du Boulay GH, McAllister VL, Marshall J, Russell RW, Symon L (1975) Cerebral blood flow in dementia. Arch Neurol 32:632–637
24. Erkinjuntti T, Inzitari D, Pantoni L, Wallin A, Scheltens P, Rockwood K, Roman GC, Chui H, Desmond DW (2000) Research criteria for subcortical vascular dementia in clinical trials. J Neural Transm (Suppl 59):23–30
25. Folstein MF, Folstein SE, McHugh PR (1975) "Mini-mental state". A practical method for grading the cognitive state of patients for the clinician. J Psychiatr Res 12:189–198
26. Kimura K, Hashikawa K, Etani H, Uehara A, Kozuka T, Moriwaki H, Isaka Y, Matsumoto M, Kamada T, Moriyama H (1990) A new apparatus for brain imaging: four-head rotating gamma camera single photon emission computed tomograph. J Nucl Med 31:603–609
27. Nagao M, Murase K, Yasuhara Y, Ikezoe J (1998) Quantitative analysis of pulmonary emphysema: three-dimensional fractal analysis of single-photon emission computed tomography images obtained with a carbon particle radioaerosol. AJR Am J Roentgenol 171:1657–1663
28. Murase K, Nagao M, Kikuchi T (1999) Three-dimensional fractal analysis for quantification of heterogeneity of radioisotope distribution in the organ using SPECT. J Nucl Med 40:292
29. Loeb C, Gandolfo C, Croce R, Conti M (1992) Dementia associated with lacunar infarction. Stroke 23:1225–1229
30. Yao H, Sadoshima S, Kuwabara Y, Ichiya Y, Fujishima M (1990) Cerebral blood flow and oxygen metabolism in patients with vascular dementia of the Binswanger type. Stroke 21:1694–1699
31. Takano T, Kimura K, Nakamura M, Fukunaga R, Kusunoki M, Etani H, Matsumoto M, Yoneda S, Abe H (1985) Effect of small deep hemispheric infarction on the ipsilateral cortical blood flow in man. Stroke 16:64–69
32. Kobayashi S, Okada K, Yamashita K (1991) Incidence of silent lacunar lesion in normal adults and its relation to cerebral blood flow and risk factors. Stroke 22:1379–1383
33. Hatazawa J, Shimosegawa E, Satoh T, Toyoshima H, Okudera T (1997) Subcortical hypoperfusion associated with asymptomatic white matter lesions on magnetic resonance imaging. Stroke 28:1944–1947
34. Loeb C (1995) Dementia due to lacunar infarctions: a misnormer or a clinical entity?. Eur Neurol 35:187–192
35. del Ser T, Bermejo F, Portera A, Arredondo JM, Bouras C, Constantinidis J (1990) Vascular dementia: A clinicopathological study. J Neurol Sci 96:1–17

36. Friston KJ, Frith CD, Liddle PF, Frackowiak RS (1991) Comparing functional (PET) images: the assessment of significant change. J Cereb Blood Flow Metab 11:690–699

37. Minoshima S, Frey KA, Koeppe RA, Foster NL, Kuhl DE (1995) A diagnostic approach in Alzheimer's disease using three-dimensional stereotactic surface projections of fluorine-18-FDG PET. J Nucl Med 36:1238–1248

38. Yamaguchi S, Meguro K, Itoh M, Hayasaka C, Shimada M, Yamazaki H, Yamadori A (1997) Decreased cortical glucose metabolism correlates with hippocampal atrophy in Alzheimer's disease as shown by MRI and PET. J Neurol Neurosurg Psychiatry 62:596–600

Circulating adhesion molecules are correlated with ultrasonic assessment of carotid plaques

Hiroyuki HASHIMOTO, Kazuo KITAGAWA, Keisuke KUWABARA, Hidetaka HOUGAKU, Toshiho OHTSUKI, Masayasu MATSUMOTO and Masatsugu HORI

Department of Internal Medicine and Therapeutics, Osaka University Graduate School of Medicine, 2-2 Yamadaoka, Suita, Osaka 565-0871, Japan

ABSTRACT

The relationship between levels of circulating intercellular cell-adhesion molecule-1 (cICAM-1) or P-selectin (cP-selectin) and the severity of carotid atherosclerosis was examined in 301 outpatients undergoing duplex ultrasonographic examination. Carotid plaque was defined as an intima-media thickness greater than 1.0 mm, and a plaque score (PS) was calculated from the plaque thickness in both carotid arteries. Multivariate analysis demonstrated significant positive associations between cICAM-1 and the number of plaques [$\beta = 0.11$; confidence interval (CI), 0.007–0.213], maximum intima-media thickness ($\beta = 0.11$; CI, 0.01–0.219), and PS ($\beta = 0.10$; CI, 0.001–0.205). In contrast, no significant association was found for cP-selectin. cP-selectin did not increase until atherosclerosis was advanced (PS > 10), showing a marked increase in patients with $\geqslant 50\%$ stenosis. The circulating levels of both proteins are related to real measurements of plaque formation in the carotid arteries independently of classical risk factors. Marked elevation of cP-selectin occurs in advanced carotid atherosclerosis after gradual elevation of cICAM-1.

INTRODUCTION

In vitro and animal experiments have demonstrated that adherence of circulating leucocytes to endothelial cells and subsequent transendothelial migration are critical steps in the early stages of atherosclerosis [1]. Recent clinical investigations have focused on the relationship between the levels of circulating leucocyte–endothelial adhesion molecules and cardiovascular disease (CVD). Among the various circulating adhesion molecules, circulating intercellular cell-adhesion molecule-1 (cICAM-1) has received the most attention, and two large-scale studies have demonstrated that an elevated cICAM-1 level is a predictor of future cardiovascular events [2,3]. With respect to other leucocyte–endothelial adhesion molecules, several experimental and histological studies have shown a close relationship between P-selectin and ICAM-1, and some studies have revealed that circulating P-selectin (cP-selectin) levels are higher in patients who suffer a subsequent cardiovascular event than in patients who do not [4–6]. Of the other circulating adhesion molecules, cP-selectin is the strongest predictor of the risk of cardiovascular events after cICAM-1 [7].

Detection of carotid atherosclerosis is useful because it is an indicator of generalized atherosclerosis [8–11] and a reliable predictor of future CVD [12–15]. However, studies investigating the relationship between circulating levels of the above adhesion molecules and carotid atherosclerosis had different population sizes and different indicators to estimate the severity of

Key words: adhesion molecule, atherosclerosis, carotid artery, circulating intercellular cell-adhesion molecule-1 (cICAM-1), circulating P-selectin (cP-selectin), inflammation, ultrasound.

Abbreviations: (c)ICAM-1, (circulating) intercellular cell-adhesion molecule-1; CI, confidence interval; cP-selectin, circulating P-selectin; HbA_{1c}, glycated haemoglobin; HDL, high-density lipoprotein; PS, plaque score; CVD, cardiovascular disease; IMT, intima-media thickness.

Correspondence: Dr Hiroyuki Hashimoto, Department of Internal Medicine, Osaka National Hospital 2-1-14, Hoenzaka, Chuoku, Osaka 540-0006, Japan (e-mail hashih@onh.go.jp).